

Interaction of silicon photonic crystal nanocavities with colloidal lead sulphide nanocrystals for enhanced spontaneous emissions near 1.55 μm at room temperature

Ranojoy Bose^(a), Xiaodong Yang, Rohit Chatterjee, Jie Gao, and Chee Wei Wong.

Optical Nanostructures Laboratory, Columbia University, New York, NY 10027

Abstract:

We observe the weak coupling of lead sulphide nanocrystals to localized defect modes of 2-dimensional silicon nanocavities through enhancement of spontaneous emission. Cavity resonances characterized with the nanocrystals agree with cold-cavity measurements using integrated waveguides, but linewidths are broadened, perhaps due to limits of resolution in measurements. Selective isolation of nanocrystals only at the cavity further suppresses background photoluminescence. The theoretical enhancement is near 7, and the calculated Purcell factor is 65. These novel light sources operate near 1.55 μm wavelengths at room temperature, permitting integration with current fiber communications networks.

(a) rb2261@columbia.edu

The study of cavity quantum electrodynamics (CQED) in wavelength-scale optical cavities is of central interest in the field of optics and solid-state physics, and has traditionally been performed with quantum dots (QD) formed through self-assembly¹⁻⁴. Single and indistinguishable photon sources¹ and strong coupling²⁻⁴ have been achieved and show great promise toward the realization of effective quantum networking and quantum computing schemes. Self-assembled quantum dots (SAQD), however, are typically in III-V semiconductors and cannot benefit from the vast and advanced silicon foundry infrastructure for large-scale integration. For silicon photonic crystals, an alternative approach is to integrate colloidal QDs after device fabrication, using spin- or drop-casting techniques⁵ as a post-processing step. This approach further benefits from the ability to synthesize nanocrystals separately to attain high-quality characteristics and for emissions at 1.55 μm wavelengths. Colloidal lead salt nanocrystal quantum dots have recently emerged as excellent candidates for charge-based as well as optical applications. The ability to synthesize these nanoparticles in various core-shells and for a variety of wavelength ranges allows for wide-ranging applications, for example, as efficient fluorescent tags in biomolecules⁶. Lead sulphide (PbS) QD, used in the experiments presented here, exhibit strong quantum confinement and stable photoluminescence in the near infrared at room temperature with high quantum yields, and have been studied in detail in literature⁷. We have proposed earlier the interactions of silicon cavities with PbS nanocrystals and explored this theoretically⁵. Colloidal nanocrystal interactions have also been reported in AlGaAs cavities at shorter wavelengths⁸, as well as in other recent CQED experiments⁹.

The theory of cavity quantum electrodynamics is documented in great detail for the case of QDs in (or near) a photonic crystal cavity. In the more common operational realm of weak coupling, cavity quality factor (Q) characterization, narrowing of the excitonic linewidth, and modification of photoluminescence lifetime have been demonstrated in accordance with theory for many different

material systems in both 1D and 2D photonic crystals. With improved nanocavity design and fabrication, the dipole-nanocavity coupling strength, approximated by the Rabi frequency g_0 , can exceed the dipole decay- and dephasing rates of the nanocrystals, as well as the cavity mode decay rates in many systems. Hence, with excellent alignment of a single QD to the field maximum of the cavity mode, strong coupling has also been remarkably observed²⁻⁴.

In the case of weak coupling, and under perfect spectral and spatial alignment, the spontaneous emission rates of the resonant excitons are modified according to the well-known Purcell factor F_p ¹⁰:

$$F_p = \frac{3\lambda^3}{4\pi^2 n^3} \frac{Q}{V_{eff}}$$

where λ is the resonant wavelength of the cavity mode and V_{eff} the interacting cavity modal volume. Hence Q/V_{eff} stands as the figure-of-merit in weak coupling QED systems and a high value is desirable as in our solid-state photonic crystal cavities. Moreover, a semiconductor solid-state approach allows interaction with the same nanocrystal or ensemble over time, in contrast to atomic cavity QED.

The enhancement in spontaneous emission for a nanocrystal emitter positioned at the maximum of the electric field intensity of the cavity field mode, and polarization-matched to the cavity field mode, is given by the expression¹¹:

$$E = F_p \times \frac{\gamma_c(2\gamma_e + \gamma_c)}{4(1 - \frac{\omega_c}{\omega_e})^2 + (2\gamma_e + \gamma_c)^2}$$

where ω_c and ω_e are the frequencies of the cavity resonance and emitter respectively, and γ_e and γ_c are the emitter and cavity decay rates respectively. In the case where the nanocrystal linewidth exceeds the cavity mode linewidth, the enhancement is dictated by V_{eff} , and a high-quality factor does not contribute significantly toward larger enhancements.

In the experiments, optimized $L3$ nanocavities¹² (three linearly missing air-holes in an otherwise periodic triangular lattice) are used, with or without an additional center hole for both mid-cavity-plane and evanescent coupling of the nanocrystals. The design parameters are as follows: $a = 420$ nm, $r = 0.29a (\pm 10\%)$, $r_c = 0.28a (\pm 10\%)$, and $t = 252$ nm where a , r , r_c , and t represent the lattice parameter, radius of holes, radius of additional center hole, and slab thickness respectively ($r_c = 0.26a (\pm 10\%)$ is also used). All cavities are $s1$ - or $s3$ - detuned¹². The photonic crystal devices are fabricated on a SiO_2 substrate and incorporate waveguides (Fig. 1, 2) that allow for lensed optical fiber-waveguide coupling and characterization of the nanocavities using radiation collection measurements¹². In this way, the coupled nanocrystal measurements can be confirmed with the radiation spectrum of the cavity field modes. The $L3$ cavity with a center hole is almost equivalent to two coupled- $L1$ nanocavities, where cavity modes are formed due to constructive or destructive interference of modes in the two cavities. The devices are characterized (Fig. 1) using 3D finite-difference time-domain (FDTD) simulations, using a freely available software package with subpixel smoothing for increased accuracy¹³. A mode-volume of approximately $0.07 \mu\text{m}^3$ is calculated for the lattice parameter listed above. This mode volume is more than twice that for an $L1$ cavity ($0.03 \mu\text{m}^3$). The designed cavity corresponds to a Purcell factor of 65. Spontaneous emission enhancements are estimated using the spatial distribution of the electric field energy densities computed at slab-center (for photonic crystal cavity with center hole) and near the surface of the slab, and equal ~ 7 at the slab-center and 4 at the slab surface. The devices are fabricated either at the Columbia cleanroom facilities using electron-beam lithography, or the Institute of Microelectronics Singapore using deep UV lithography with 270 nm critical dimension resolution. Scanning electron microscope (SEM) images show a high quality of fabrication (Fig. 2).

PbS nanocrystals are used as a broad-band light source to decorate the resonant mode(s) of the 2D silicon photonic crystal resonator. The nanocrystals, obtained commercially through Evidot Technologies., exhibit high photoluminescence efficiency and room temperature stability. The nanocrystals are obtained in a mixture of polymethylmethacrylate (PMMA; 5-15% by weight) and toluene (85-95% by weight) and exhibit a room temperature photoluminescence peak around 1500 nm, with a full-width half-maximum of 100-150 nm. The emission peak is sensitive to temperature. After diluting the commercially obtained sample 2:3 parts by volume in toluene, an overall thin-film of approximately 100 nm is achieved at a spin rate of 5000 rpm. For larger film-thicknesses, radiation from the cavity-coupled nanocrystals is covered under background photoluminescence from the uncoupled nanocrystals. A QD density of 10^3 per μm^2 is estimated.

The 100-nm thin-film of PMMA ($n=1.56$) changes the band structure of the photonic crystal device⁸ and shifts the cavity resonance as well as the spatial electric field profile of the cavity mode due a changed index contrast, but these changes can be effectively monitored experimentally due to the presence of waveguides on the devices. It is not clear whether the PMMA infiltrates the holes of the silicon photonic crystal. The spectrum from cavity field modes with a thin-film of PMMA is shown in Fig. 3. For some devices, excess PMMA is also selectively removed from regions away from the cavity using electron-beam lithography to suppress background photoluminescence in measurements.

PbS nanocrystals near the cavity are excited off-resonance using a pulsed Ti:S laser operating around 800 nm with a repetition rate of 80 MHz, pulse duration of 150 fs and average power of 800 mW. The pump signal reaching the nanocrystals is attenuated. The laser light is reflected by a high-pass filter and a 60X objective lens is used to focus the beam. The radiation from the cavity is collected with the same objective lens from a spot less than 5 μm in diameter, dispersed by a 32 cm

JY Horiba Triax 320 monochromator, and detected using a liquid nitrogen cooled Ge detector. An additional high-pass filter is used near the monochromator slit to filter out any signal from the Ti:S laser.

Waveguide characterization of the cavity modes is performed in the same setup by using a tapered lens fiber coupled to an on-chip waveguide. In this case, an ANDO tunable laser source operating between 1480 nm and 1580 nm at 8 mW peak power is used. Cavity Q of between 500 and 1000 is estimated from the radiation spectrum for different cavity designs, after the QD have been spin-coated (Fig. 3).

The collection path is set up by aligning to the cavity radiation using an infrared camera and an ASE broadband laser source for fiber-based excitation. Once this path is established, the Ti:S laser is used to pump the nanocrystals. Figure 4 shows the results of the coupling measurements. Enhancement is observed at the cavity, compared to a spot approximately 10 μm away, where the photoluminescence spectrum follows the familiar Gaussian lineshape with a full-width half-maximum of around 100 nm. Photoluminescence from uncoupled nanocrystals can be further suppressed by using a polarizer in the collection path. The measurements are confirmed with fiber-based characterization of the devices. However, in the measurements, the individual peaks in the radiation spectrum (Fig. 3) are not resolved, and a broader enhanced peak is observed, centered at a cavity mode. This broadening may partly be attributed to the resolution used in the coupling measurements (> 3 nm, owing to very low signal levels from the QD), but may also be effected by the large homogeneous linewidths of coupled PbS nanocrystals, although the latter is not theoretically confirmed.

In silicon-based photonic crystal cavity systems, we observe, for the first time to our knowledge, the enhanced spontaneous emission of colloidal PbS nanocrystals at the near-infrared and at room

temperature, following earlier theoretical suggestions⁵. The operation of the coupled nanocavity-nanocrystal system in silicon at around 1550 nm is especially promising because of the possibility of a single photon source that can be integrated into the present fiber infrastructure and the scalability with silicon CMOS foundries. This is an alternative to the remarkable CQED experiments performed and suggested elsewhere^{14, 15}.

[The authors acknowledge funding support from the Columbia University Initiatives in Science and Engineering in Nanophotonics, the Department of Mechanical Engineering, the shared experimental facilities and cleanroom that are supported by the MRSEC and NSEC Programs of the National Science Foundation (DMR-0213574) and by the New York State Office of Science, Technology and Academic Research. The measured devices were fabricated at the Columbia cleanroom as well as the Institute of Microelectronics, from which we acknowledge the support of Dr. Dim-Lee Kwong and Dr. Mingbin Yu. The authors also thank helpful discussions with Dr. Tomoyuki Yoshie, Dirk Englund, and Dr. Dmitri Talapin, and assistance from Somil Mehta].

Figure Captions

Fig. 1. (a) FDTD visualization of silicon photonic crystal with air holes, with integrated waveguide for fiber-based characterization, (b) E_x field profile of cavity mode at slab center for designed photonic crystal device, computed with 3D FDTD. (c) Enhancement computed with FDTD for the same mode.

Fig. 2. Scanning electron microscope images of fabricated silicon devices. (a) $s3$ with detunings of $0.176a$, $0.025a$ and $0.176a$ for the three holes adjacent to the cavity, center hole of radius $0.308a$, (b) no hole at $L3$ cavity center. (c) Angled view of typical SOI device. Scale bar represents $2\text{ }\mu\text{m}$ in (a) and (b) and $1\text{ }\mu\text{m}$ in (c). $r = 0.319a$.

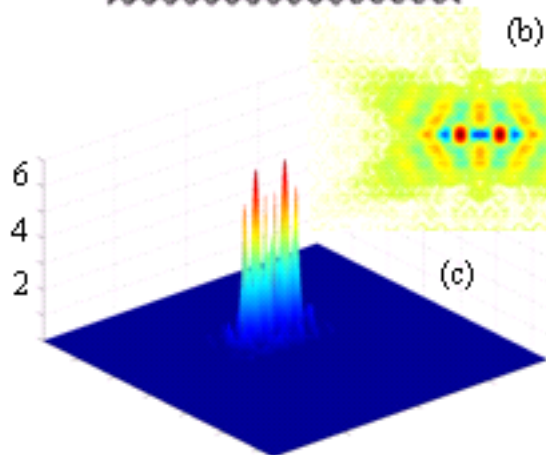
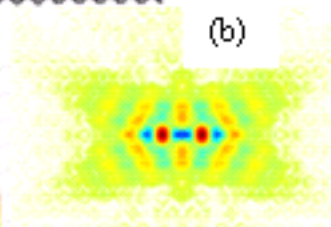
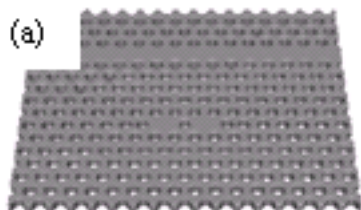
Fig. 3. Cavity transmission characterized using a tunable laser after 100 nm PMMA coating for (a) $L3$ nanocavity with $s3$ detuning and center-hole of radius $0.308a$; (b) cavity with $s1$ detuning ($.176a$) and center-hole radius $0.308a$, after selective PMMA removal; and (c) cavity with $s1$ detuning and center-hole radius of $0.286a$. $r = 0.319a$.

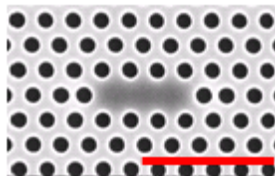
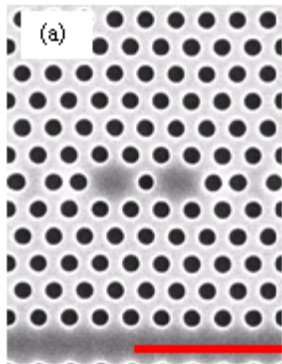
Fig. 4. Coupling measurements: (a) Photoluminescence from uncoupled QD; (b) coupling corresponding to cavity in Fig. 3a; (c) coupling corresponding to cavity in Fig. 3b; and (d) coupling corresponding to cavity in Fig. 3c. The pump fluence is approximately $10\text{ }\mu\text{J}/\text{cm}^2$.

References

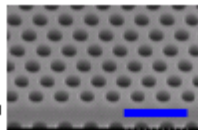
- [1] D. Englund, D. Fattal, E. Waks, G. Solomon, B. Zhang, T. Nakaoka, Y. Arakawa, Y. Yamamoto, and J. Vučković, *Phys. Rev. Lett.* **95**, 013904 (2005)
- [2] T. Yoshie, A. Scherer, J. Hendrickson, G. Khitrova, H. M. Gibbs, G. Rupper, C. Ell, O. B. Shchekin, and D. G. Deppe, *Nature* **432**, 200 (2004)
- [3] J. P. Reithmaier, G. Sęk, A. Löffler, C. Hofmann, S. Kuhn, S. Reitzenstein, L. V. Keldysh, V. D. Kulakovskii, T. L. Reinecke, and A. Forchel, *Nature* **432**, 197 (2004)
- [4] E. Peter, P. Senellart, D. Martrou, A. Llemaître, J. Hours, J. M. Gerard, and J. Bloch, *Phys. Rev. Lett.* **95**, 067401 (2005)
- [5] R. Bose, D. V. Talapin, X. Yang, R. J. Harniman, P. T. Nguyen, and C. W. Wong, *Proc. SPIE* **6005**, 600509 (2005)
- [6] M. Bruchez Jr., M. Moronne, P. Gin, S. Weiss, A. P. Alivisatos, *Science* **281**, 2013 (1998)
- [7] I. Kang, F. W. Wise, *J. Opt. Soc. Am. B* **14**, 1632 (1997)
- [8] I. Fushman, D. Englund and J. Vučković, *Appl. Phys. Lett.* **87**, 241102 (2005)
- [9] S. Hoogland, V. Sukhovatkin, I. Howard, S. Cauchi, L. Levina, E. H. Sargent, *Opt. Exp.* **14**, 3273 (2006)
- [10] E. M Purcell, *Phys. Rev.* **69**, 681 (1946)
- [11] H. Y. Ryu and M. Notomi, *Opt. Lett.* **28**, 2390 (2003)
- [12] Y. Akahane, T. Asano, B. Song, and S. Noda, *Opt. Exp.* **13**, 1202 (2005)
- [13] A. Farjadpour, D. Roundy, A. Rodriguez, M. Ibanescu, P. Bermel, J. D. Joannopoulos, S. G. Johnson, and G. Burr, *Optics Letters*, in press (2006)
- [14] S. David, M. El kurdi, P. Boucaud, A. Chelnokov, V. Le Thanh, D. Bouchier, and J.-M. Lourtioz, *Appl. Phys. Lett.* **83**, 2509 (2003)

[15] M. Makarova, J. Vučković, H. Sanda, Y. Nishi, *arXiv: physics/0609060* (2006)





(b)



(c)

